Relativistic electron spin motion in cycloatoms

Q. Su, P.J. Peverly, R.E. Wagner, P. Krekora* and R. Grobe

Intense Laser Physics Theory Unit and Department of Physics
Illinois State University, Normal, IL 61790-4560 USA
qcsu@ilstu.edu

*   *Permanent address: Institute of Physics PAN, Al. Lotnikow 32/46, 02-668 Warsaw, Poland*

http://www.phy.ilstu.edu/ILP

Abstract: We present computer movies of the classical and quantum mechanical time evolution for an atom in a strong static magnetic field and a laser field. The resonantly induced relativistic motion of the atomic electron leads to a ring-like spatial probability density called a cycloatom. We further demonstrate that spin-orbit coupling for a fast moving electron in a cycloatom becomes significant, modifying the time-dependence of the spin even if initially aligned parallel to the static magnetic field direction. We also present several movies on time-evolution of the spin-distribution as a function of the position for a relativistic quantum state. The nature of such a space resolved spin measurement is analyzed.

©2001 Optical Society of America

OCIS codes: (000.1600) Classical and quantum physics; (020.4180) Multiphoton processes

References and links

1. For a review, see e.g. Q. Su and R. Grobe, "Examples of classical and genuinely quantum relativistic phenomena," in Multiphoton Processes, eds. L.F. DiMauro, R.R. Freeman, K.C. Kulander (American Institute of Physics, Melville, New York, 2000) p.655 or the website www.phy.ilstu.edu/ILP
2. Science News, "Ring around the proton," **157**, 287 (2000).
3. R.E. Wagner, Q. Su and R. Grobe, "Relativistic resonances in combined magnetic and laser field," Phys. Rev. Lett., **84**, 3282 (2000).
4. For movies of cycloatoms see Phys. Rev. Focus, "Fast electrons on the cheap", **5**, 15, 6 April (2000) at the web site: http://focus.aps.org/v5/st15.html story
5. P.J. Peverly, R.E. Wagner, Q. Su and R. Grobe, "Fractional resonances in relativistic magnetic-laser-atom interactions," Laser Phys. **10**, 303 (2000).
6. Q. Su, R.E. Wagner, P.J. Peverly and R. Grobe, "Spatial electron clouds at fractional and multiple magneto-optical resonances," in Frontiers of Laser Physics and Quantum Optics, eds, Z. Xu, S. Xie, S.-Y. Zhu and M.O. Scully, p.117 (Springer, Berlin, 2000).
7. R.E. Wagner, P.J. Peverly, Q. Su and R. Grobe, "Classical versus quantum dynamics for a driven relativistic oscillator," Phys. Rev. A **61**, 35402 (2000).
8. V.G. Bagrov and D.M. Gitman, *Exact solutions of relativistic wave equations*, (Kluwer Academic, Dordrecht, 1990).
9. C. Bottcher and M.R. Strayer, "Relativistic theory of fermions and classical fields on a collocation lattice," Ann. Phys. NY **175**, 64 (1987).
10. J.C. Wells, A.S. Umar, V.E. Oberacker, C. Bottcher, M.R. Strayer, J.-S. Wu, J. Drake and R. Flanery, "A numerical implementation of the Dirac equation on a hypercube multicomputer," Int. J. Mod. Phys. C **4**, 459 (1993).
11. K. Momberger, A. Belkacem and A.H. Sorensen, "Numerical treatment of the time-dependent Dirac equation in momentum space for atomic processes in relativistic heavy-ion collisions," Phys. Rev. A **53**, 1605 (1996).
12. U.W. Rathe, C.H. Keitel, M. Protopapas, and P.L. Knight, "Intense laser-atom dynamics with the two-dimensional Dirac equation," J. Phys. B **30**, L531 (1997).
13. N.J. Kylstra, A.M. Ermolaev and C.J. Joachain, "Relativistic effects in the time evolution of a one-dimensional model atom in an intense laser field," J. Phys. B **30**, L449 (1997).
14. C. Szymanowski, C.H. Keitel and A. Maquet, "Influence of Zitterbewegung on relativistic harmonic generation," Las. Phys. **9**, 133 (1999).
15. J.W. Braun, Q. Su and R. Grobe, "Numerical approach to solve the time-dependent Dirac equation," Phys. Rev. A **59**, 604 (1999).
16. U.W. Rathe, P. Sanders, P.L. Knight,"A case study in scalability: an ADI method for the two-dimensional time-dependent Dirac equation," Parallel Computing, **25**, 525 (1999).

17. P. Krekora, R.E. Wagner, Q. Su and R. Grobe, "Dirac theory of ring-shaped electron distributions." Phys. Rev. A, in press.
18. H. Goldstein, *Classical Mechanics*, 2nd edition (Addison-Wesley, New York, 1980).
19. B. Thaller, *The Dirac Equation*, (Springer, 1992).
20. R.E. Wagner, Q. Su and R. Grobe, "High-order harmonic generation in relativistic ionization of magnetically dressed atoms," Phys. Rev. A, **60**, 3233 (1999).
21. For relativistic suppression of wave packet spreading, see, Q. Su, B.A. Smetanko and R. Grobe, "Wave packet motion in relativistic electric fields," Las. Phys. **8**, 93 (1998).
22. Q. Su, B.A. Smetanko and R. Grobe, "Relativistic suppression of wave packet spreading," Opt. Express **2**, 277 (1998), http://www.opticsexpres.org/oearchive/source/2813.htm
23. E. Lenz, M. Dörr and W. Sandner, Las. Phys., in press.
24. For a review on Lorentz transformations of 4×4 spin matrices, see, e.g., J.D. Bjorken and S.D. Drell, "Relativistic quantum mechanics," (McGraw-Hill, 1964); J. Kessler, Polarized Electrons, 2nd edition (Springer Verlag, Berlin, 1985).
25. For work on the Spin-Wigner function, see, e.g., I. Bialynicki-Birula, P. Gornicki and J. Rafelski, " Phase-space structure of the Dirac vacuum," Phys. Rev. D **44**, 1825 (1991).
26. G.R. Shin, I. Bialynicki-Birula and J. Rafelski, " Wigner function of relativistic spin-1/2 particles," Phys. Rev. D **46**, 645 (1992).
27. For the time-evolution of the spatial width, see, J.C. Csesznegi, G.H. Rutherford, Q. Su, and R. Grobe, "Dynamics of wave packets in inhomogeneous and homogeneous magnetic fields," Las. Phys. **6**, 41 (1999).
28. P. Krekora, Q. Su and R. Grobe, "Dynamical signature in spatial spin distributions of relativistic electrons," Phys. Rev. A, submitted.
29. L.T. Thomas, Phil. Mag. **3**, 1 (1927).
30. J.D. Jackson, *Classical Electrodynamics* (Wiley, New York, 1999).

1. Introduction

In this paper we discuss the new quantum mechanical simulations of the relativistic electron state in atoms, referred to as cycloatoms, and explore the possibility of using the electron spin as a measure of the velocity distribution for a single quantum state. This work is part of an ongoing effort in search of genuinely relativistic quantum phenomena in strong laser fields. [1] The work is computationally intensive. The calculated data are best visualized in the form of colorful movies as shown below.

A new method to excite atoms into relativistic orbits has been proposed recently. [2,3] It is based on exploiting cyclotron-type resonances of the electron interacting with a combined laser and magnetic field. In general, a resonant excitation to relativistic speeds is typically avoided by the nonlinearity of the atomic potential encountered by the large amplitude motion. This limitation typically sets in at velocity scales much smaller than the speed of light. However, for our case of an electron in a sufficiently strong magnetic field, nonlinear atomic effects are not so important, and the velocity can grow to extremely large values until relativistic effects that limit the speed from growing beyond bound become important. In this regime a wide variety of novel relativistic phenomena have been investigated. [2,3] The electronic charge distribution, for instance, can develop into ring [4], figure-eight [5] and propeller-like structures [6] whose centers rotate around the nucleus. These relativistic charge cloud distributions (named cycloatoms) emerge from initial atomic states after a few laser cycles. The absence of cycloatoms in the corresponding non-relativistic solution for the same parameters demonstrates that this ring-structure is a genuinely relativistic phenomenon although a Coulombic non-linearity can also lead to similar structures in certain cases. To understand the formation of cycloatoms, a simplified model based on the spiral orbits of individual classical trajectories was proposed which associates the relativistic dephasing with a velocity dispersion and a non-linear mass increase enhanced by the resonance between the magnetic and laser fields.[2,3]

2. Numerical methods

The original prediction of cyclatoms was based on solutions to the Liouville equation for the classical phase space density. [2,3] It is important to determine whether these classical predictions agree with the exact solutions of the corresponding relativistic quantum system.

A first insight into the question about the applicability of classical mechanics for relativistic systems has been provided in a recent work, in which the probability density for a one-dimensional harmonic oscillator from the Dirac equation turned out to be remarkably similar to the spatial density distribution from the relativistic Liouville equation despite the inherent nonlinearity due to relativity. [7]

Wave function solutions to the time-dependent Dirac equation for atoms in external fields are difficult to obtain analytically; for a few exceptions see [8]. To overcome this technical limitation and to obtain some first insights into the relativistic dynamics, numerical solutions have been studied.   This computational challenge is at the forefront of computational physics and has been taken in the study of relativistic heavy ion collisions [9-11] and in the interaction of atoms with intense laser fields [12-16]. However, the limitations due to the finite amount of CPU time and memory, even on the fastest supercomputers, are severe and restrict the accessible parameter regime that can be studied today.

The classical dynamics is governed by the relativistic Liouville equation [18] (in atomic units)

$$\frac{\partial \rho(\mathbf{r},\mathbf{p},t)}{\partial t} = \left\{ \sqrt{c^4 + c^2 \left(\mathbf{p} + \frac{1}{c} \mathbf{A}(\mathbf{r},t) \right)^2 } + V(\mathbf{r}), \; \rho(\mathbf{r},\mathbf{p},t) \right\}_{\mathbf{r},\mathbf{p}} \qquad (1)$$

for the phase space density $\rho(\mathbf{r},\mathbf{p},t)$. Here $\{...\}_{\mathbf{r},\mathbf{p}}$ denotes the Poisson brackets with respect to the phase space variables, $V(\mathbf{r})=-(r^2+1)^{-1/2}$ is the smoothed Coulomb potential, and c is the speed of light. In this paper we use two different vector potentials, the first one, $\mathbf{A}(\mathbf{r},t) = -$ E $c/\omega_L \sin(\omega_L t) \, \mathbf{e}_x + (\Omega \, \mathbf{e}_z) \times \mathbf{r}/2$ represents the linearly polarized laser field along the x-direction and the static magnetic field Ω is along the z-direction. The second one, $\mathbf{A}(\mathbf{r},t) = c$ E t $\mathbf{e}_x$, represents a static electric field along the negative x-direction.

Equation (1) is solved numerically via a Monte-Carlo technique typically based on 50,000 particle orbits. The corresponding spatial probability distribution can be obtained via $P_{cl}(\mathbf{r},t) = \int d\mathbf{p} \, \rho(\mathbf{r},\mathbf{p},t)$. None of the phenomena discussed here are very sensitive to the details of the initial state which is chosen as $\rho(\mathbf{r}, \; \mathbf{p}, \; t=0) \; = \frac{1}{\pi^2} \exp[-(\mathbf{r}/\Delta x_0)^2/2]$ $\exp[-2(\mathbf{p}\,\Delta x_0)^2]$ and is centered at the origin with a spatial width Δx_0.

The classical distribution $P_{cl}(\mathbf{r},t)$ will be compared directly with the corresponding quantum mechanical density $P_{qm}(\mathbf{r},t) = \sum_{i=1}^{4} |\Psi_i(\mathbf{r},t)|^2$, where the summation extends over the four spinor components.   The wave function $\Psi(\mathbf{r},t)$ can be obtained from the corresponding numerical solution to the Dirac equation:

$$i \frac{\partial}{\partial t} \Psi(\mathbf{r},t) \; = \left[c\boldsymbol{\alpha} \left(\mathbf{p} + \frac{1}{c} \mathbf{A}(\mathbf{r},t) \right) + \boldsymbol{\beta} c^2 + V(\mathbf{r}) \right] \Psi(\mathbf{r},t) \qquad (2)$$

where $\boldsymbol{\alpha}$ and $\boldsymbol{\beta}$ denote the 4×4 Dirac matrices [19]. The time-dependent wave function $\Psi(\mathbf{r},t)$ can be calculated on a space-time grid using a recently developed split-operator algorithm based on a fast Fourier transformation that is accurate up to the fifth order in time [15]. In all of the simulations presented below, the one or two spatial axes are discretized into 65,536 grid points which together with up to 45,000 temporal points per laser cycle lead to converged results with an overall error of less than 5%.

To have an initial quantum mechanical state that is closest to the classical density used above we have chosen $\Psi(\mathbf{r},t=0) = (2\pi\Delta x_0^2)^{-3/4} \exp[-(\mathbf{r}/\Delta x_0)^2/4] \, \Phi_{x,z}$. We used $\Phi_x = (1,1,0,0)/\sqrt{2}$ and $\Phi_z = (1,0,0,0)$ to represent initial spin states with averages $\langle S_x(t=0) \rangle = 1/2$ a.u. and $\langle S_z(t=0) \rangle = 1/2$ a.u., respectively.

3. Quantum analogue of the classical cycloatom electron distribution?

In Fig. 1 the system is characterized by a cyclotron frequency Ω=96 a.u., a laser field amplitude of E=800 a.u. and a frequency ω_L =80 a.u.. The combined magnetic and laser field accelerates the electron to 44% of the speed of light after 4 laser cycles. We should note that due to the relativistic resonance shifts discussed in [2,3,5,6,20], the maximum speed obtained in the corresponding non-relativistic calculation is only v=0.33 c. This is quite counter-intuitive in that relativistic effects normally lead to a less-accelerated and less rapid motion that can be associated with a nonlinear mass increase.
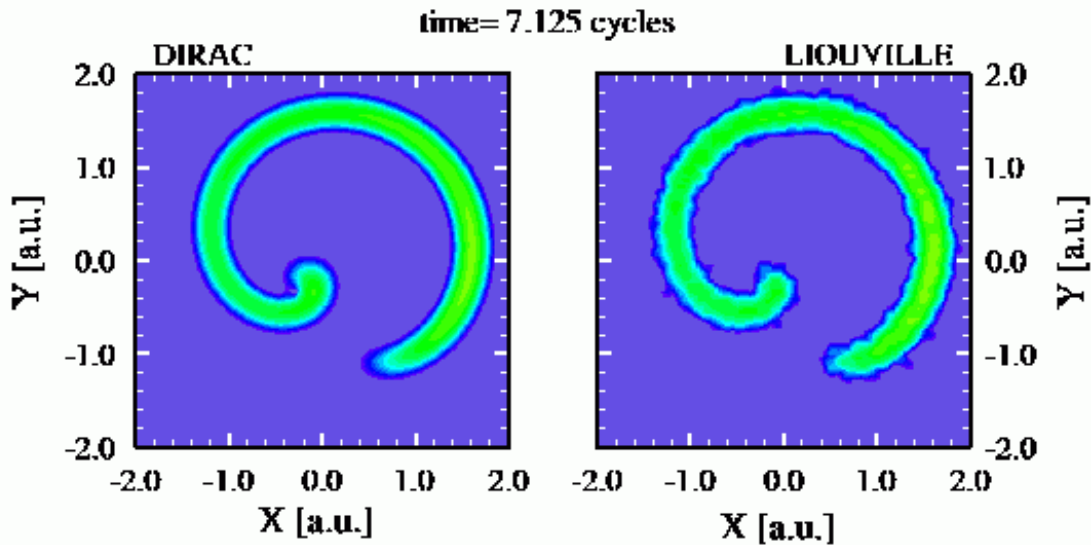
Fig. 1   The formation of cycloatoms. Please click to play the movie. [2.1 MB]

In Fig. 1 we compare the time evolution of the classical with the quantum mechanical spatial probability density as a function of time. The left graph is the exact solution of the Dirac equation $\sum_{i=1}^{4} |\Psi_i(x,y,t)|^2$, and the right graph shows the solution of the relativistic Liouville equation. The wave packet with an initial width Δx_0=0.1 a.u. develops after a few laser oscillations into a "banana-like" shape that evolves into a ring. The center of this ring-structure follows a circular orbit around the nucleus with the laser period. [17] The agreement between the classical and quantum descriptions is remarkable. The jagged contour lines at the edges of the ring in the classical density are a small numerical artifact due to the discreteness of the individual trajectories.

4. Position-dependent spin densities

Before we explore the spin information from the electron probability density distribution shown in Fig. 1, we first show how the relativistic Lorentz contraction of the spin due to large orbital speeds can lead to a position-dependent spin density. To illustrate this effect in its purest form without any other spin-coupling we first discuss the simplest possible case of an electron that is accelerated in a static electric field: $\mathbf{A}(\mathbf{r},t) = cEt\mathbf{e}_x$.

Fig. 2 displays the time evolution of the electron's spatial probability density along the x-axis for E=300 a.u. As the electron accelerates along the x-axis it spreads spatially until

its speed approaches c. In that limit the spreading is relativistically suppressed and the wave packet develops into a slightly asymmetric form. [21-23]
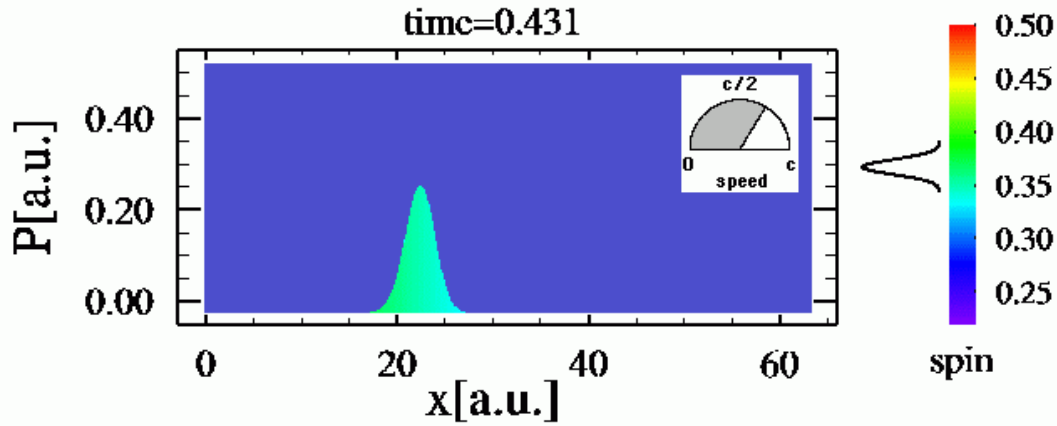
Fig. 2   Spatial and spin density for an electron wave packet accelerated by a static electric field. [960 k]

Before we discuss the color gradation used in the movie. to represent the spin density, let us comment on the spin averages, which are not shown. The average value of spin along the propagation axis $<S_x(t)>$ is practically constant, whereas the spin perpendicular to the x-axis ($<S_z(t)>$) decays as the electron's speed increases. This decay is associated with the Lorentz spin contraction which is different from the Lorentz length contraction in that the perpendicular component rather than the parallel component is affected by the relativistic motion. The spin decay can be understood if we perform a Lorentz transformation into the electron's rest frame in which the spin remains constant if the negative energy components in the state are not significant. The spin, when observed from the lab frame, (in which the Dirac equation is solved) appears to be contracted by the Lorentz-gamma factor,

$$\langle\!\langle \mathbf{S}(\mathbf{v})\rangle\!\rangle = [1 - (\mathbf{v}_\perp / c)^2]^{1/2} \langle\!\langle \mathbf{S}(\mathbf{v}=0)\rangle\!\rangle \qquad (3)$$

where $\mathbf{v}_\perp$ denotes the velocity component perpendicular to the spin vector $\mathbf{S}$. [24]

Next we will return to the question of how the spatial spin distribution (color gradation) was computed for the movie. We define a "position-dependent spin variable" as $\mathbf{S}(\mathbf{r},t) \equiv \Psi^\dagger(\mathbf{r},t)\mathbf{S}\Psi(\mathbf{r},t) / \Psi^\dagger(\mathbf{r},t)\Psi(\mathbf{r},t)$. This quantity matches well the corresponding spatial spin distribution for a classical ensemble of spins. It is the average value of the spin one would measure if the electron were detected at time t at location r. [25,26] Please note that the reference to the word "average" is used in a quantum statistical sense; any individual spin measurement, of course, leads to $\pm 1/2$ a.u. From this definition it follows that $< \mathbf{S}(t)> = <\Psi(\mathbf{r},t) \mid \mathbf{S} \mid \Psi(\mathbf{r},t)> = \iiint dx\, dy\, dz\, \mathbf{S}(\mathbf{r},t)\, P(\mathbf{r},t)$, where $P(\mathbf{r},t) = \Psi^\dagger(\mathbf{r},t)\Psi(\mathbf{r},t)$ is the usual spatial probability density, given by the sum of the four squared spinor components of the wave function.

In Fig. 2 we display the spin distributions $S_z(x,t)$ by using different colors. Red corresponds to $S_z(x,t)=+1/2$ and dark blue to $S_z(x,t)=0$. The corresponding distribution $S_x(x,t)$ along the direction of propagation remains spatially as well as temporally constant, $S_x(x,t)=1/2$ a.u.. Initially, the state was in a spin eigenstate, and is not shown since it remains one throughout the time evolution. In other words, the spin operator S_x commutes with the Dirac Hamiltonian in one spatial direction, and the momentum eigenstates with velocities along the x-direction are also spin S_x eigenstates. For a direction perpendicular to the x-direction, the situation is different; the spin is not associated with a "good" quantum number

for a wave packet and $S_z(x,t)$ decreases as a function of time and space. It is quite interesting to note that in addition to the overall lowered spin value as time increases, the spatial spin distribution becomes non-uniform. The spins associated with the front-edge of the accelerated wave packet are relatively smaller (more "blueish"), reflecting the fact that the larger velocity components of the wave packet have traveled to the right edge of the quantum state. One can almost view the spin distribution $S_z(x,t)$ as a spatially resolved "speedometer" for the quantum mechanical state in this case.

We have also calculated a "classical" spin distribution from the classical Liouville phase-space density $\rho(\mathbf{r},\mathbf{p},t)$ via:

$$S_z^{class}(\mathbf{r},t) = \int d\mathbf{p} \frac{1}{2}\sqrt{1-(\mathbf{v}_\perp(\mathbf{p})/c)^2}\,\rho(\mathbf{r},\mathbf{p},t) \qquad (4)$$

It is practically indistinguishable from the exact Dirac spin distribution. This perfect agreement demonstrates that some kinetic aspects of the spin dynamics can be approximated quite well by concepts of classical (relativistic) mechanics.

5. Spin-densities of cycloatoms

Before we discuss the dynamics of the spin-densities for cycloatoms, let us first describe the spins for the simpler system of an electron wave packet in a static magnetic field without the laser field [27] for the non-relativistic case. Using non-relativistic orbital analysis with direct field-spin coupling, the iso-spin lines for the spin distribution $S_z^{class}(x,y,t)$ are concentric circles of various radii. In contrast to these circles, the iso-spin lines for the distribution $S_x^{class}(x,y,t)$ are straight lines with a time-dependent slope of $-[1-\cos(\Omega t)]/\sin(\Omega t)$.

Let us now return to the most complicated case for which the dynamics of the spins is governed by a velocity-dependent cyclotron (Larmor) frequency and the Lorentz contraction, which is a function of the relativistic orbital motion. The left picture of Fig. 3 shows $S_z(r,t)$.

The spin distributions are displayed only for those spatial regions for which the probability density $\Psi^\dagger(r,t)\,\Psi(r,t)$ exceeds 6×10^{-6}. It has been recorded for the same parameters as Fig. 1. At early times, the packet is non-relativistic and we see the concentric ring-like contour lines reminiscent of those of the non-relativistic orbits. [28] The region around the origin has the smallest velocity contributions and therefore the smallest amount of Lorentz contraction. It is quite remarkable that even at later times (t> 0.4 a.u.), when the tail end begins to curve inward towards the origin, the spin contour lines in the front edge of the growing tail still approximately follow the simple concentric circles. At later times when the tail end has closed the distribution to a full circle at time t= 0.6 a.u., the front tail again contains very small velocity contributions. This increase and decrease of the Lorentz contraction associated with different spatial parts of the distribution can be directly associated with outward (accelerating) and inward going (decelerating) spiral orbits associated with the classical dephasing model. As a result the spin distribution $S_z(r,t)$ seems to depend mainly on the specific position and not so much on time.
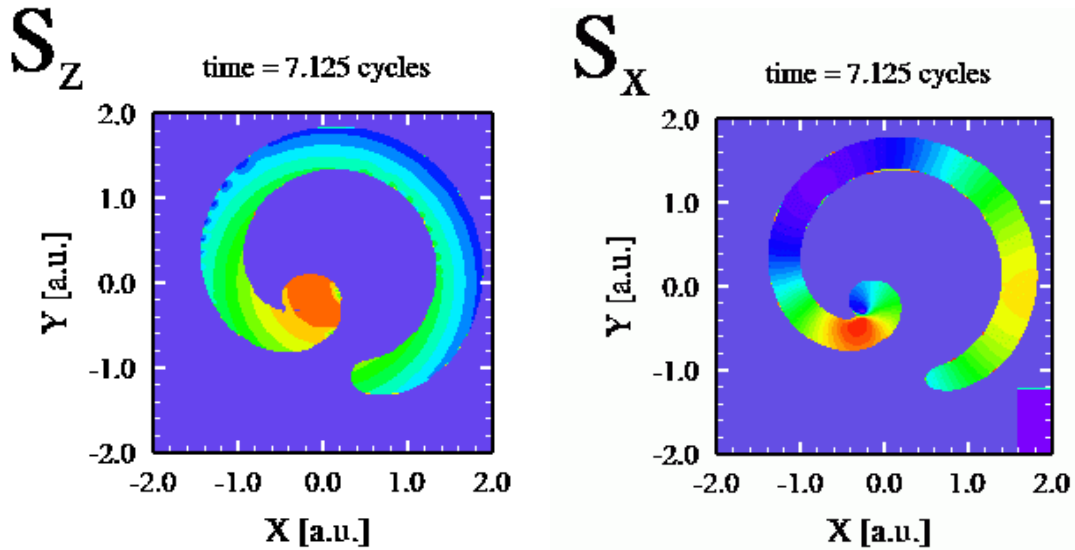
Fig. 3   Spatial spin distribution in relativistic cycloatoms. [2.3 MB]

In the right frame of the movie we display the corresponding spin-distribution S_x for an initial state with $S_x(r,t=0)=1/2$ a.u.   It is the result of three independent relativistic effects. The first one is the Lorentz contraction, which restricts the maximum spin value and depends only on the instantaneous velocity in the y-direction v_y.   The second effect is due to the relativistic mass-shift, leading effectively to a velocity dependent Larmor frequency; this effect is accumulative in the sense that the entire history of different Larmor frequencies contribute to the phase and the amplitude of the local spin value. A third effect is the well-known Thomas precession, [29,30] whose frequency for a uniformly accelerated system is given by $\omega_T=(\gamma-1)$ $a\times v/v^2$. Approximating the acceleration $|a|$ with $v\Omega$ and assuming an average value of $v=c/4$ for the speed, the Thomas precession frequency $|(\gamma-1)\Omega|$ would amount to $\Omega/31.5$, which is much smaller than the cyclotron frequency and corresponds for our parameters to a time even longer than the total duration of interaction. As the final state is the result of all of these accumulative and non-accumulative effects, we discuss the impact of these effects step by step as the electron becomes relativistic.

To better focus on the impact of relativity on the Larmor precession, we have indicated in the lower right box the value of a function $1/2 \cos(\Omega t)$ associated with a (spatially constant, but time-dependent) spin density of a wave packet for which the spin is (artificially) decoupled from the orbital motion for each frame. In contrast to $S_z(r,t)$ the spin contour lines for $S_x(r,t)$ are not concentric circles. If the spin were only affected by the Lorentz effect, we would expect parallel lines. [18] However, in addition to this effect, the faster contributions in the leading tail experience a smaller effective Larmor frequency. As a result, the spin value lags behind the (spin-orbital decoupled) value of $1/2 \cos(\Omega t)$. This effect curves the otherwise parallel contour lines. The snapshot at time t= 4.08 T nicely illustrates both effects. Here T = $2\pi/\omega_L$ is the laser period. The distribution at the center and the tail end are out of phase but they have the same spin value. As the spins get out of phase in a continuous manner along the distribution one could expect somewhere a maximum spin value of 1/2 a.u. However, in this case the maximum value is associated with the left most part of the distribution [$(x,y) \approx (-1,0)$ a.u.] where the velocity v_y is largest. As a result the Lorentz contraction forbids the maximum value of 1/2 in this region. A similar effect can be observed at later times t= 9.36 T when the spins of the front end and those close to the origin are completely out of phase. Here the maximum spin value 1/2 a.u. is taken at the upper part of the distribution where the Lorentz

contraction is negligible ($v_y \approx 0$). We note that the contour lines recorded at the largest time $t=$ 9.36 T are along straight lines; all of which seem to originate at various locations close to the origin.

In summary, we have shown that the predictions of cycloatoms based on classical mechanics are confirmed by the Dirac theory. A direct comparison of the quantum with the classical counterparts does not reveal any major difference in the relativistic domain. Furthermore, this resonance regime reveals an interesting spatial spin distribution which may be associated with the coupling between the spin and the orbital motion. We proposed the spin as a measure for the velocity distribution in the relativistic quantum state.